ACS APPLIED MATERIALS & INTERFACES

www.acsami.org Research Article

Auger Suppression of Incandescence in Individual Suspended Carbon Nanotube pn-Junctions

Bo Wang, Sisi Yang, Yu Wang, Ragib Ahsan, Xiaowei He, Younghee Kim, Han Htoon, Rehan Kapadia, Demis D. John, Brian Thibeault, Stephen K. Doorn, and Stephen B. Cronin*

Cite This: https://dx.doi.org/10.1021/acsami.9b17519 Read Online

ACCESS | Metrics & More | Article Recommendations | Supporting Information

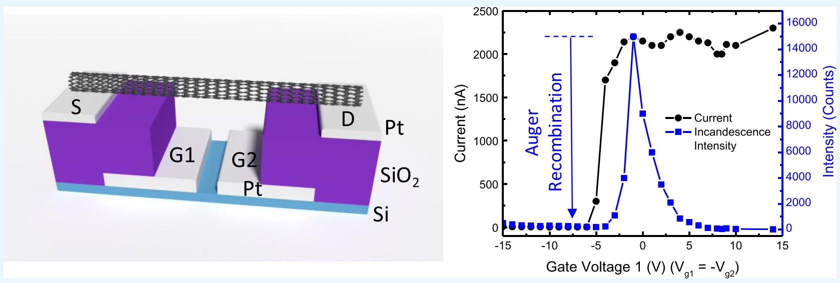

ABSTRACT: There are various mechanisms of light emission in carbon nanotubes (CNTs), which give rise to a wide range of spectral characteristics that provide important information. Here we report suppression of incandescence via Auger recombination in suspended carbon nanotube pn-junctions generated from dual-gate CNT field-effect transistor (FET) devices. By applying equal and opposite voltages to the gate electrodes (i.e., $V_{g1} = -V_{g2}$), we create a pn-junction within the CNT. Under these gating conditions, we observe a sharp peak in the incandescence intensity around zero applied gate voltage, where the intrinsic region has the largest spatial extent. Here, the emission occurs under high electrical power densities of around 0.1 MW/cm^2 (or 6 μW) and arises from thermal emission at elevated temperatures above 800 K (i.e., incandescence). It is somewhat surprising that this thermal emission intensity is so sensitive to the gating conditions, and we observe a 1000-fold suppression of light emission between V_{g1} = 0 and 15 V, over a range in which the electrical power dissipated in the nanotube is roughly constant. This behavior is understood on the basis of Auger recombination, which suppresses light emission by the excitation of free carriers. Based on the calculated carrier density and band profiles, the length of the intrinsic region drops by a factor of 7−25× over the range from $|V_g|$ = 0 to 15 V. We, therefore, conclude that the light emission intensity is significantly dependent on the free carrier density profile and the size of the intrinsic region in these CNT devices.

KEYWORDS: *high-field, ballistic, band-to-band, avalanche, photon emission, photoemission*

INTRODUCTION

Light emission from nanoscale devices (i.e., III−V semiconducting quantum dots and carbon nanotubes (CNTs)) exhibits interesting optoelectronic and optical phenomena, including localized exciton-based light emission, room-temperature single-photon emission, and trions.[1−11] The IBM group first reported electrically driven light emission from on-substrate single CNT pn-junctions[12−14] with a relative efficiency of light emission around 10^{-4} photon/pair of injected electrons and holes. After that, electrically driven light emission was reported from several CNT field-effect transistor (FET) devices by several groups.[15−25] In these studies, detectable light emission was only achieved at relatively high applied electrical powers, above 1 μW. Under these cases, significant Joule heating occurs, as evidenced by Raman G band frequency shifts,[15,26−29] and it has become clear that, in these previous works, Joule heating caused thermal emission as the main mechanism of light emission. Additionally, electrically driven light emission from silicon-based pn-junctions and FETs was also reported.[30−33] Other than FET-based devices, electrically driven light emission was also reported using other approaches, including asymmetric contacts and arrays of aligned CNTs.[34−38] Under very high electric fields (0.5 MV/cm), light emission via avalanche breakdown was also reported in air-suspended CNT FETs.[29,39,40] Under these conditions, the light emission efficiencies were much higher (three orders of magnitude) than former reports of electrically driven light emission in the

Received: November 8, 2019
Accepted: February 21, 2020
Published: February 21, 2020

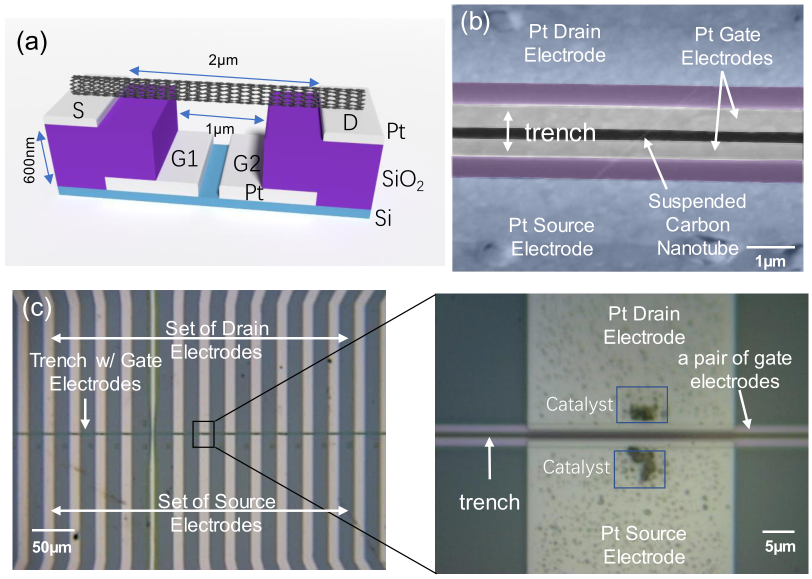

Figure 1. (a) Schematic diagram, (b) colorized scanning electron microscope (SEM) image, and (c) optical microscope images of a dual-gate suspended carbon nanotube field-effect transistor.

literature, and the G band frequency was monitored to rule out thermal emission explicitly.[15,26−28]

In the work presented here, we explore the incandescence characteristics of dual-gated CNTs as the pn-junction is swept from reverse bias to forward bias. Before any light-emitting diode (LED)-like light emission can be observed (i.e., reaches the light emission detection limit), the incandescence becomes extremely significant due to high electrical power density and consequent heating. While no LED-like light emission is observed, clear signatures of avalanche emission and thermal emission are seen, including an interesting peak around zero gate voltage (i.e., $V_{g1} = -V_{g2} \approx 0$). To the best of our knowledge, this is the only system where the incandescence (i.e., thermal emission) intensity can be tuned by electrostatic doping, while the electrical power (i.e., device temperature) is held constant. An incandescence spectrum is collected around the peak point to corroborate the broadband thermal emission.

■ RESULTS AND DISCUSSION

Figure 1a shows the suspended dual-gate CNT field-effect transistor (FET) device used in this work. Two separate platinum (Pt) gate electrodes shared by 29 pairs of drain and source electrodes are first deposited on a high-resistivity silicon wafer. Then, on top of the silicon, an approximately 600 nm thick SiO_2 layer is grown using plasma-enhanced chemical vapor deposition (PECVD). A trench 1000 nm wide and 600 nm deep is etched through the SiO_2 layer using dry etching (reactive-ion etching, RIE). Photolithography is then used to deposit 29 pairs of drain and source Pt electrodes on the surface of the wafer. The gap between the drain and source Pt electrodes is 2 μm, the suspended length is 1 μm, and the gap between gates is 200 nm. Figure 1b shows a colorized scanning electron microscope (SEM) image of a suspended CNT across drain and source electrodes. Optical microscope images of a representative dual-gate CNT FET chip are shown in Figure 1c.[41−43] To deposit the $Fe(NO_3)_3/Al_2O_3$-based catalyst, lithographically defined windows (5×5 μm^2) are written on the drain and source Pt electrodes in a photoresist layer. The final step of the device fabrication is CNT growth, using argon and hydrogen gas bubbled through ethanol with high purity at 825 °C, via a homebuilt chemical vapor deposition (CVD) system.[44] The devices were electrically characterized using a semiconductor measurement unit system. Here we ground the drain electrode for all of the electric measurement processes, while the bias voltage is applied to the source. Incandescence images are taken with an InGaAs camera (Xenics, Inc), which is thermoelectrically cooled and provides a sensitivity over the 1000−1600 nm wavelength range. The Xenics software is capable of reading light intensities from a selected area or a pixel within the incandescence images. Photoluminescence and incandescence spectra are collected using the same homebuilt spectrometer system with an InGaAs array (Princeton Instruments, Inc), which is sensitive over the same effective wavelength range as our imaging detector. A 785 nm continuous wave (CW) laser with a power of 0.2 mW is used in the NIR spectrometer system.

Figure 2a,b shows a 1100 nm wavelength illuminated image and an incandescence image of a dual-gate CNT FET using an InGaAs camera. Here, incandescence occurs under applied gate voltages of $V_{g1} = 2$ V, $V_{g2} = -2$ V and a current of $I = 2.2$ μA at a bias voltage of $V_{bias} = 3.5$ V. Figure 2c shows the incandescence intensity (blue curve) and the electric current (black curve) plotted as a function of gate voltage 1 (i.e., V_{g1}) with opposite and equal gate voltages (i.e., $V_{g1} = -V_{g2}$) and keeping the bias voltage at a constant value of 3.5 V. While the electrical current and power remain almost constant over the range -3 V $\leq V_{g1} \leq 10$ V ($P \approx 6$ μW), the incandescence intensity exhibits a peak around $V_{g1} = -V_{g2} = 0$. A plot of the G band Raman frequency as a function of gate voltage taken from a typical dual-gate CNT FET has been added in the Supporting Information document as Figure S7. Under conditions when the applied current is larger than 1 μA, substantial downshifts are shown (>10 cm^{-1}), which corresponds to temperatures above 800 K based on a coefficient of around 0.02 cm^{-1}/K.[27,45] Here we observe a 1000-fold suppression in the incandescence intensity between $V_{g1} = 0$ and 15 V. Moreover, the light emission intensity is asymmetric with respect to positive and negative gate voltages

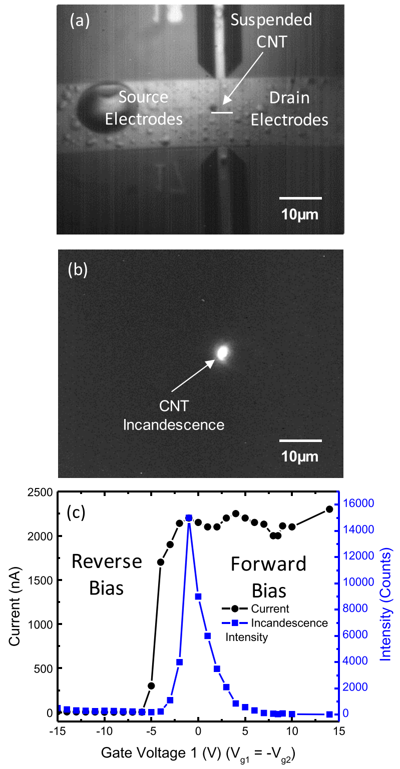

Figure 2. (a, b) IR image with illumination and incandescence image (without illumination) from a suspended dual-gate CNT FET device taken with an InGaAs camera. (c) Current and incandescence intensity plotted as a function of gate voltage 1 with $V_{g1} = -V_{g2}$ and V_{bias} = 3 V.

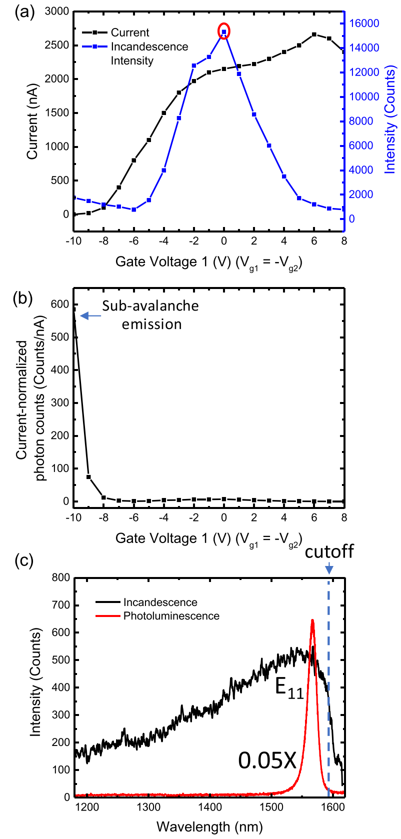

Figure 3. (a) Current and incandescence intensity plotted as a function of gate voltage 1 with $V_{g1} = -V_{g2}$ and V_{bias} = 3 V. (b) Current-normalized photon counts plotted as a function of gate voltage 1 with $V_{g1} = -V_{g2}$ and V_{bias} = 3 V. (c) Incandescence spectrum taken at the red-circled point indicated in (a) and photoluminescence spectrum taken from the same dual-gate CNT FET device.

(i.e., forward and reverse bias), consistent with the simulation results shown below in Figure 4.

Figure 3a plots the current (black curve) and incandescence intensity (blue curve) as a function of gate voltage (V_{g1}) for another device, which exhibits similar behavior to that shown in Figure 2c. Here, the two gate voltages are again equal and opposite (i.e., $V_{g1} = -V_{g2}$), and the bias voltage is held at a constant value of +3 V. Here, the data is plotted across a narrower gate voltage range ($-10 \leq V_{g1} \leq +8$) than the device shown in Figure 2. Figure 3b plots the current-normalized photon counts (counts/current) as a function of gate voltage. Here, we should note that, although the light intensity plot shows a sharp peak around zero gate voltage, the relative efficiency of subavalanche emission at $V_{g1} = -V_{g2} = -10$ V (570 counts/nA) is much higher than that at the peak point around zero gate voltage, which is around 10 counts/nA. This result agrees with our previous report that the efficiency of subavalanche (i.e., impact ionization) emission is substantially higher than that of thermal emission.[29,39] Figure 3c shows the spectra of photoluminescence and incandescence taken at V_b = +3 V, $I = 2$ μA, and $V_{g1} = 0$, which exhibits a broad (thermally broadened) band gap emission corresponding to E_{11} exciton. It should be noted that, when V_{g1} is negative with a corresponding current of less than 10 nA, the device becomes reverse biased and subavalanche emission appears due to impact ionization.

We hypothesize that this peak around zero gate voltage (shown in Figures 2c and 3a) appears when Auger recombination in the nanotube is minimized, particularly in the suspended region of the nanotube. At finite gate voltages, the gate-induced carriers are known to reduce the emission efficiency via Auger recombination, which is a nonradiative process.[46−49] This presents a mechanism by which the light emission efficiency is reduced by more than one order of magnitude as the intrinsic width becomes smaller. It is interesting to note that, in both Figures 2c and 3a, the intensity peak occurs at only zero gate voltage. This stands in contrast to previous reports of photoluminescence quenching by Yasukochi et al. in which the intensity peak extends over a range of voltages around zero gating.[48] While we do not fully understand this dissimilar behavior, there are several differences between this device configuration. Namely, our device is a dual-gate pn-junction rather than a single-gate device. Also, our intensity profile was obtained under high bias conditions and hence high temperatures of ∼800 K. Lastly, incandescence and photoluminescence are fundamentally different processes and can potentially be affected differently by the Auger recombination mechanism, and there are likely different competing recombination mechanisms that dominate under these gate and bias conditions.

To further understand the underlying Auger suppression of the incandescence intensity observed in these pn-devices around zero gate voltage, we simulated the valence and conduction band profiles and carrier density profiles along the length of the CNT under various gate voltages and a constant bias voltage via a self-consistent Poisson solver in the TCAD Sentaurus software package.[50] Figure 4a shows the valence and

https://dx.doi.org/10.1021/acsami.9b17519
ACS Appl. Mater. Interfaces XXXX, XXX, XXX−XXX

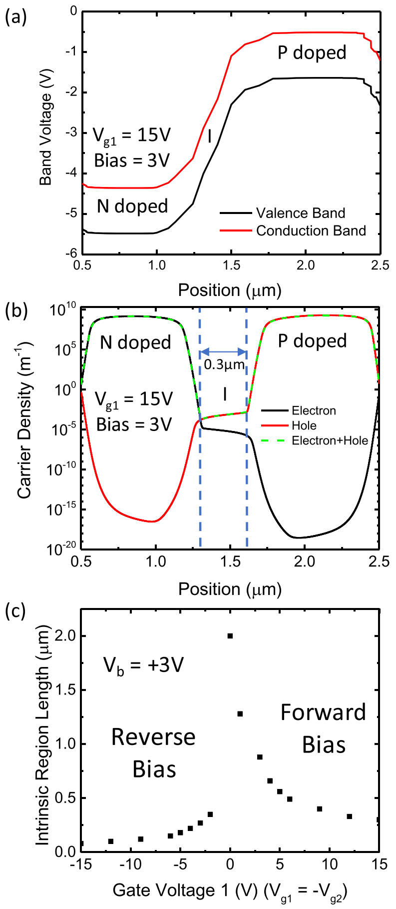

Figure 4. (a) Calculated conduction and valence band profiles and (b) calculated carrier density profiles of a dual-gate CNT FET device at $V_{g1} = -V_{g2} = 15$ V under a bias voltage of 3 V. (c) Width of the intrinsic region plotted as a function of applied gate voltage with $V_{g1} = -V_{g2}$ at $V_b = 3$ V.

conduction band profiles along the device, and Figure 4b shows a semilog plot of the carrier density profiles at $V_{g1} = -V_{g2} = 15$ V under a bias voltage of 3 V. Here we find that the size of the intrinsic region drops by a factor of 7−25× over the range from $|V_g| = 0$ to 15 V, as shown in Figure 4c ($V_b = 3$ V). Also, the voltage dependence of the length of the intrinsic region (i.e., minimal Auger recombination) closely resembles the incandescence intensity profiles of Figures 2c and 3a. Even the gate voltage-dependent asymmetry can be seen in the measured (Figure 2c) and calculated (Figure 4c) results, indicating that, under forward bias, the intrinsic region extends further than under reverse bias. We, therefore, conclude that the suppressed light emission intensity is caused by the decreased width of the intrinsic region in these CNT devices around zero gate voltage. Additional valence and conduction band profiles and the corresponding carrier density profiles are included in the Supporting Information document, further supporting the mechanism of light emission suppression via Auger recombination.

CONCLUSIONS

We report a suppression behavior in the incandescence of suspended CNT dual-gated pn-devices. Here, the peak around zero gate voltage arises from the alignment of the intrinsic region of the pn-junction with the trench. It is somewhat surprising that this thermal emission intensity is so sensitive to the gating conditions, and we observe a 1000-fold suppression due to Auger recombination between $V_{g1} = 0$ and 15 V at nearly constant electrical power. This alignment suppresses thermal emission from the device by increasing Auger recombination. That is, Auger recombination (i.e., non-radiative recombination) suppresses light emission under high gating conditions. From the calculated carrier density and band profiles, a strong correlation is established between incandescence intensity and the size of the intrinsic region, consistent with the Auger recombination mechanism.

ASSOCIATED CONTENT

Supporting Information

The Supporting Information is available free of charge at https://pubs.acs.org/doi/10.1021/acsami.9b17519.

Calculated valence and conduction band profiles; carrier density profiles; electric field profiles; $I-V$ curves, and G band Raman spectra (PDF)

AUTHOR INFORMATION

Corresponding Author

Stephen B. Cronin − *Department of Physics and Astronomy and Ming Hsieh Department of Electrical Engineering, University of Southern California, Los Angeles, California 90089, United States;* orcid.org/0000-0001-9153-7687; Email: scronin@usc.edu

Authors

Bo Wang − *Department of Physics and Astronomy, University of Southern California, Los Angeles, California 90089, United States*

Sisi Yang − *Department of Physics and Astronomy, University of Southern California, Los Angeles, California 90089, United States;* orcid.org/0000-0003-0352-833X

Yu Wang − *Mork Family Department of Chemical Engineering and Materials Science, University of Southern California, Los Angeles, California 90089, United States*

Ragib Ahsan − *Ming Hsieh Department of Electrical Engineering, University of Southern California, Los Angeles, California 90089, United States;* orcid.org/0000-0002-3833-7851

Xiaowei He − *Center for Integrated Nanotechnologies, Materials Physics and Applications Division, Los Alamos National Laboratory, Los Alamos, New Mexico 87545, United States;* orcid.org/0000-0002-4982-8250

Younghee Kim − *Center for Integrated Nanotechnologies, Materials Physics and Applications Division, Los Alamos National Laboratory, Los Alamos, New Mexico 87545, United States;* orcid.org/0000-0002-4499-3783

Han Htoon − *Center for Integrated Nanotechnologies, Materials Physics and Applications Division, Los Alamos National Laboratory, Los Alamos, New Mexico 87545, United States;* orcid.org/0000-0003-3696-2896

Rehan Kapadia − *Ming Hsieh Department of Electrical Engineering, University of Southern California, Los Angeles, California 90089, United States;* orcid.org/0000-0002-7611-0551

Demis D. John − *Nanotech, Department of Electrical and Computer Engineering, University of California Santa Barbara, Santa Barbara, California 93106, United States*

https://dx.doi.org/10.1021/acsami.9b17519
ACS Appl. Mater. Interfaces XXXX, XXX, XXX−XXX

Brian Thibeault − *Nanotech, Department of Electrical and Computer Engineering, University of California Santa Barbara, Santa Barbara, California 93106, United States*

Stephen K. Doorn − *Center for Integrated Nanotechnologies, Materials Physics and Applications Division, Los Alamos National Laboratory, Los Alamos, New Mexico 87545, United States;* orcid.org/0000-0002-9535-2062

Complete contact information is available at: https://pubs.acs.org/10.1021/acsami.9b17519

Notes

The authors declare no competing financial interest.

ACKNOWLEDGMENTS

The authors would like to acknowledge support from the Northrop Grumman-Institute of Optical Nanomaterials and Nanophotonics (NG-ION^2) (B.W.). This research was supported by the NSF Award no. CBET-1905357 (S.Y.), Department of Energy DOE Award no. DE-FG02-07ER46376 (Y.W.), and USC Provost Fellowship (R.A.). A portion of this work was carried out at the University of California Santa Barbara (UCSB) nanofabrication facility. This work was also carried out in part at the Center for Integrated Nanotechnologies, a U.S. Department of Energy, Office of Science user facility. Y.L., S.K.D., and H.H. acknowledge the partial support of the LANL LDRD program and Y.K. and H.H. acknowledge support from DOE BES FWP# LANLBES22.

REFERENCES

(1) Matsunaga, R.; Matsuda, K.; Kanemitsu, Y. Observation of Charged Excitons in Hole-Doped Carbon Nanotubes Using Photoluminescence and Absorption Spectroscopy. *Phys. Rev. Lett.* **2011**, *106*, No. 037404.

(2) Yuma, B.; Berciaud, S.; Besbas, J.; Shaver, J.; Santos, S.; Ghosh, S.; Weisman, R. B.; Cognet, L.; Gallart, M.; Ziegler, M.; Honerlage, B.; Lounis, B.; Gilliot, P. Biexciton, Single Carrier, and Trion Generation Dynamics in Single-Walled Carbon Nanotubes. *Phys. Rev. B* **2013**, *87*, No. 205412.

(3) Högele, A.; Galland, C.; Winger, M.; Imamoglu, A. Photon Antibunching in the Photoluminescence Spectra of A Single Carbon Nanotube. *Phys. Rev. Lett.* **2008**, *100*, No. 217401.

(4) He, X. W.; Hartmann, N. F.; Ma, X. D.; Kim, Y.; Ihly, R.; Blackburn, J. L.; Gao, W. L.; Kono, J.; Yomogida, Y.; Hirano, A.; Tanaka, T.; Kataura, H.; Htoon, H.; Doorn, S. K. Tunable Room-Temperature Single-Photon Emission at Telecom Wavelengths from SP(3) Defects in Carbon Nanotubes. *Nat. Photonics* **2017**, *11*, 577−582.

(5) Ghosh, S.; Bachilo, S. M.; Simonette, R. A.; Beckingham, K. M.; Weisman, R. B. Oxygen Doping Modifies Near-Infrared Band Gaps in Fluorescent Single-Walled Carbon Nanotubes. *Science* **2010**, *330*, 1656−1659.

(6) Miyauchi, Y.; Iwamura, M.; Mouri, S.; Kawazoe, T.; Ohtsu, M.; Matsuda, K. Brightening of Excitons in Carbon Nanotubes on Dimensionality Modification. *Nat. Photonics* **2013**, *7*, 715−719.

(7) Ma, X.; Adamska, L.; Yamaguchi, H.; Yalcin, S. E.; Tretiak, S.; Doorn, S. K.; Htoon, H. Electronic Structure and Chemical Nature of Oxygen Dopant States in Carbon Nanotubes. *ACS Nano* **2014**, *8*, 10782−10789.

(8) Ma, X. D.; Baldwin, J.K.S.; Hartmann, N. F.; Doorn, S. K.; Htoon, H. Solid-State Approach for Fabrication of Photostable, Oxygen-Doped Carbon Nanotubes. *Adv. Funct. Mater.* **2015**, *25*, 6157−6164.

(9) Ma, X.; James, A. R.; Hartmann, N. F.; Baldwin, J. K.; Dominguez, J.; Sinclair, M. B.; Luk, T. S.; Wolf, O.; Liu, S.; Doorn, S. K.; Htoon, H.; Brener, I. Solitary Oxygen Dopant Emission from Carbon Nanotubes Modified by Dielectric Metasurfaces. *ACS Nano* **2017**, *11*, 6431−6439.

(10) Ishii, A.; Uda, T.; Kato, Y. K. Room-Temperature Single-Photon Emission from Micrometer-Long Air-Suspended Carbon Nanotubes. *Phys. Rev. Appl.* **2017**, *8*, 54039.

(11) Ma, X. D.; Hartmann, N. F.; Baldwin, J.K.S.; Doorn, S. K.; Htoon, H. Room-Temperature Single-Photon Generation from Solitary Dopants of Carbon Nanotubes. *Nat. Nanotechnol.* **2015**, *10*, 671−675.

(12) Mueller, T.; Kinoshita, M.; Steiner, M.; Perebeinos, V.; Bol, A. A.; Farmer, D. B.; Avouris, P. Efficient Narrow-Band Light Emission from A Single Carbon Nanotube P-N Diode. *Nat. Nanotechnol.* **2010**, *5*, 27−31.

(13) Misewich, J. A.; Martel, R.; Avouris, P.; Tsang, J. C.; Heinze, S.; Tersoff, J. Electrically Induced Optical Emission from A Carbon Nanotube FET. *Science* **2003**, *300*, 783−786.

(14) Lee, K. G.; Chen, X. W.; Eghlidi, H.; Kukura, P.; Lettow, R.; Renn, A.; Sandoghdar, V.; Götzinger, S. A Planar Dielectric Antenna for Directional Single-Photon Emission and Near-Unity Collection Efficiency. *Nat. Photonics* **2011**, *5*, 166−169.

(15) Liu, Z. W.; Bushmaker, A.; Aykol, M.; Cronin, S. B. Thermal Emission Spectra from Individual Suspended Carbon Nanotubes. *ACS Nano* **2011**, *5*, 4634−4640.

(16) Adam, E.; Aguirre, C. M.; Marty, L.; St-Antoine, B. C.; Meunier, F.; Desjardins, P.; Menard, D.; Martel, R. Electroluminescence from Single-Wall Carbon Nanotube Network Transistors. *Nano Lett.* **2008**, *8*, 2351−2355.

(17) Zaumseil, J.; Ho, X. N.; Guest, J. R.; Wiederrecht, G. P.; Rogers, J. A. Electroluminescence from Electrolyte-Gated Carbon Nanotube Field-Effect Transistors. *ACS Nano* **2009**, *3*, 2225−2234.

(18) Pfeiffer, M.H.P.; Sturzl, N.; Marquardt, C. W.; Engel, M.; Dehm, S.; Hennrich, F.; Kappes, M. M.; Lemmer, U.; Krupke, R. Electroluminescence from Chirality-sorted (9,7)-Semiconducting Carbon Nanotube Devices. *Opt. Express* **2011**, *19*, A1184−A1189.

(19) Freitag, M.; Perebeinos, V.; Chen, J.; Stein, A.; Tsang, J. C.; Misewich, J. A.; Martel, R.; Avouris, P. Hot Carrier Electroluminescence from A Single Carbon Nanotube. *Nano Lett.* **2004**, *4*, 1063−1066.

(20) Chen, J.; Perebeinos, V.; Freitag, M.; Tsang, J.; Fu, Q.; Liu, J.; Avouris, P. Bright Infrared Emission from Electrically Induced Excitons in Carbon Canotubes. *Science* **2005**, *310*, 1171−1174.

(21) Mann, D.; Kato, Y. K.; Kinkhabwala, A.; Pop, E.; Cao, J.; Wang, X. R.; Zhang, L.; Wang, Q.; Guo, J.; Dai, H. J. Electrically Driven Thermal Light Emission from Individual Single-Walled Carbon Nanotubes. *Nat. Nanotechnol.* **2007**, *2*, 33−38.

(22) Xie, L. M.; Farhat, H.; Son, H. B.; Zhang, J.; Dresselhaus, M. S.; Kong, J.; Liu, Z. F. Electroluminescence from Suspended and On-Substrate Metallic Single-Walled Carbon Nanotubes. *Nano Lett.* **2009**, *9*, 1747−1751.

(23) Wang, S.; Zeng, Q. S.; Yang, L. J.; Zhang, Z. Y.; Wang, Z. X.; Pei, T. A.; Ding, L.; Liang, X. L.; Gao, M.; Li, Y.; Peng, L. M. High-Performance Carbon Nanotube Light-Emitting Diodes with Asymmetric Contacts. *Nano Lett.* **2011**, *11*, 23−29.

(24) Jakubka, F.; Grimm, S. B.; Zakharko, Y.; Gannott, F.; Zaumseil, J. Trion Electroluminescence from Semiconducting Carbon Nanotubes. *ACS Nano* **2014**, *8*, 8477−8486.

(25) Higashide, N.; Yoshida, M.; Uda, T.; Ishii, A.; Kato, Y. K. Cold Exciton Electroluminescence from Air-Suspended Carbon Nanotube Split-Gate Devices. *Appl. Phys. Lett.* **2017**, *110*, No. 191101.

(26) Bushmaker, A. W.; Deshpande, V. V.; Bockrath, M. W.; Cronin, S. B. Direct Observation of Mode Selective Electron-Phonon Coupling in Suspended Carbon Nanotubes. *Nano Lett.* **2007**, *7*, 3618−3622.

(27) Hsu, I. K.; Pettes, M. T.; Aykol, M.; Shi, L.; Cronin, S. B. The Effect of Gas Environment on Electrical Heating in Suspended Carbon Nanotubes. *J. Appl. Phys.* **2010**, *108*, No. 084307.

(28) Amer, M.; Bushmaker, A.; Cronin, S. Anomalous Kink Behavior in the Current-Voltage Characteristics of Suspended Carbon Nanotubes. *Nano Res.* **2012**, *5*, 172−180.

(29) Wang, B.; Rezaeifar, F.; Chen, J. H.; Yang, S.; Kapadia, R. S.; Cronin, S. B. Avalanche Photoemission in Suspended Carbon Nanotubes: Light without Heat. *ACS Photonics* **2017**, *4*, 2706−2710.
(30) Xu, K.; Huang, L.; Zhang, Z.; Zhao, J.; Zhang, Z.; Snyman, L.; Swart, J. Light Emission from A Poly-Silicon Device with Carrier Injection Engineering. *Mater. Sci. Eng. B* **2018**, *231*, 28−31.
(31) Xu, K.; Chen, Y.; Okhai, T. A.; Snyman, L. W. Micro Optical Sensors Based on Avalanching Silicon Light-Emitting Devices Monolithically Integrated on Chips. *Opt. Mater. Express* **2019**, *9*, 3985−3997.
(32) Xu, K. Silicon MOS Optoelectronic Micro-Nano Structure Based on Reverse-Biased PN Junction. *Phys. Status Solidi A* **2019**, *216*, No. 1800868.
(33) Kuai, S.; Meldrum, A. High-Speed Color-Switching Silicon LEDs. *Adv. Mater.* **2008**, *20*, 3844−3847.
(34) Khasminskaya, S.; Pyatkov, F.; Flavel, B. S.; Pernice, W. H.; Krupke, R. Waveguide-Integrated Light-Emitting Carbon Nanotubes. *Adv. Mater.* **2014**, *26*, 3465−3472.
(35) Yu, D.; Wang, S.; Ye, L.; Li, W.; Zhang, Z.; Chen, Y.; Zhang, J.; Peng, L.-M. Electroluminescence from Serpentine Carbon Nanotube Based Light-Emitting Diodes on Quartz. *Small* **2014**, *10*, 1050−1056.
(36) Xie, X.; Islam, A. E.; Wahab, M. A.; Ye, L. N.; Ho, X. N.; Alam, M. A.; Rogers, J. A. Electroluminescence in Aligned Arrays of Single-Wall Carbon Nanotubes with Asymmetric Contacts. *ACS Nano* **2012**, *6*, 7981−7988.
(37) Graf, A.; Murawski, C.; Zakharko, Y.; Zaumseil, J.; Gather, M. C. Infrared Organic Light-Emitting Diodes with Carbon Nanotube Emitters. *Adv. Mater.* **2018**, *30*, No. 1706711.
(38) Wang, R.; Wu, H.; Chen, R.; Chi, Y. Strong Electrochemiluminescence Emission from Oxidized Multiwalled Carbon Nanotubes. *Small* **2019**, No. 1901550.
(39) Wang, B.; Yang, S.; Shen, L.; Cronin, S. B. Ultra-Low Power Light Emission via Avalanche and Sub-Avalanche Breakdown in Suspended Carbon Nanotubes. *ACS Photonics* **2018**, *5*, 4432−4436.
(40) Banerjee, S.; Wong, S. S. Synthesis and Characterization of Carbon Nanotube−Nanocrystal Heterostructures. *Nano Lett.* **2002**, *2*, 195−200.
(41) Bushmaker, A. W.; Deshpande, V. V.; Hsieh, S.; Bockrath, M. W.; Cronin, S. B. Direct Observation of Born-Oppenheimer Approximation Breakdown in Carbon Nanotubes. *Nano Lett.* **2009**, *9*, 607−611.
(42) Bushmaker, A. W.; Deshpande, V. V.; Hsieh, S.; Bockrath, M. W.; Cronin, S. B. Large Modulations in the Intensity of Raman-Scattered Light from Pristine Carbon Nanotubes. *Phys. Rev. Lett.* **2009**, *103*, 67401.
(43) Chang, S. W.; Theiss, J.; Hazra, J.; Aykol, M.; Kapadia, R.; Cronin, S. B. Photocurrent Spectroscopy of Exciton and Free Particle Optical Transitions in Suspended Carbon Nanotube pn-junctions. *Appl. Phys. Lett.* **2015**, *107*, No. 053107.
(44) Deshpande, V. V.; Chandra, B.; Caldwell, R.; Novikov, D. S.; Hone, J.; Bockrath, M. Mott Insulating State in Ultraclean Carbon Nanotubes. *Science* **2009**, *323*, 106−110.
(45) Hsu, I. K.; Kumar, R.; Bushmaker, A.; Cronin, S. B.; Pettes, M. T.; Shi, L.; Brintlinger, T.; Fuhrer, M. S.; Cumings, J. Optical Measurement of Thermal Transport in Suspended Carbon Nanotubes. *Appl. Phys. Lett.* **2008**, *92*, No. 063119.
(46) Freitag, M.; Steiner, M.; Naumov, A.; Small, J. P.; Bol, A. A.; Perebeinos, V.; Avouris, P. Carbon Nanotube Photo- and Electroluminescence in Longitudinal Electric Fields. *ACS Nano* **2009**, *3*, 3744−3748.
(47) Steiner, M.; Freitag, M.; Perebeinos, V.; Naumov, A.; Small, J. P.; Bol, A. A.; Avouris, P. Gate-Variable Light Absorption and Emission in a Semiconducting Carbon Nanotube. *Nano Lett.* **2009**, *9*, 3477−3481.
(48) Yasukochi, S.; Murai, T.; Moritsubo, S.; Shimada, T.; Chiashi, S.; Maruyama, S.; Kato, Y. K. Gate-Induced Blueshift and Quenching of Photoluminescence in Suspended Single-Walled Carbon Nanotubes. *Phys. Rev. B* **2011**, *84*, No. 121409.
(49) Yoshida, M.; Popert, A.; Kato, Y. K. Gate-Voltage Induced Trions in Suspended Carbon Nanotubes. *Phys. Rev. B* **2016**, *93*, No. 041402.
(50) *50Sentaurus, T. C. A. D.*; version l-2016, Synopsys Inc.: Mountain View, CA, USA, 2016.

https://dx.doi.org/10.1021/acsami.9b17519
ACS Appl. Mater. Interfaces XXXX, XXX, XXX−XXX